Study of Tau Decays with Neutral Kaons using the L3 Detector at LEP

M. Biasini[a], L3 collaboration

[a]CERN European Organization for Nuclear Research, PPE Division
CH-1211 GENEVE 23, Switzerland

We present the study of one-prong τ decays with neutral kaons in the final state. Using the data sample collected by the L3 detector at LEP in 1991, 1992 and 1993, corresponding to an integrated luminosity of $69pb^{-1}$, we have measured the branching fractions for the following decays: $\tau^- \rightarrow \nu_\tau\pi^-\bar{\mathrm{K}}^0$, $\tau^- \rightarrow \nu_\tau\pi^-\pi^0\bar{\mathrm{K}}^0$ and $\tau^- \rightarrow \nu_\tau\pi^-\mathrm{K}^0\bar{\mathrm{K}}^0$.

Introduction

The measurement of the branching fractions of τ decays with neutral kaons are important for understanding τ decays, in particular they can provide new information on the dynamics of neutral kaon production which is not yet well understood [1].

Using the fine-grained hadron calorimeter of L3, the following decay modes have been studied: $\nu_\tau\pi^-\bar{\mathrm{K}}^0$, $\nu_\tau\pi^-\pi^0\bar{\mathrm{K}}^0$, and $\nu_\tau\pi^-\mathrm{K}^0\bar{\mathrm{K}}^0$. The L3 detector is well suited to this measurement as the efficiencies for detection of the $\mathrm{K_L}$ and $\mathrm{K_S}$ components of K^0 are comparable due to the small decay volume [2].

The data sample used in this analysis corresponds to an integrated luminosity of $69pb^{-1}$ collected at $\sqrt{s} \approx M_\mathrm{Z}$ during the 1991, 1992 and 1993 LEP running periods.

Selection of τ Decays with Neutral Kaons

The L3 detector is described in detail in reference [3]. The $\mathrm{e^+e^-}$ collision point is surrounded by a tracking chamber (TEC), a high resolution electromagnetic calorimeter (BGO), a cylindrical shell of scintillation counters, a hadron calorimeter (HCAL), and a muon chamber system. The detector is installed in a large magnet providing a uniform 0.5 Tesla field. The fine-grained hadron calorimeter of L3 [4] is used to detect neutral kaons and to measure their energies and directions. The selection of τ decays with neutral kaons is based on the coincidence of high energy deposition in the hadron calorimeter and a low momentum charged track detected in the central tracker.

The selection of Z decays into τ pairs is described in detail in reference [5]. To select an event for the $\tau^- \rightarrow \nu_\tau\mathrm{K}^0\mathrm{X}^-$ channel, exactly one charged track is required in the hemisphere defined by the plane perpendicular to the thrust axis of the event. In order to select neutral kaons, a significant excess of energy in the hadron calorimeter is required, with respect to the deposition expected from the charged track. The energy deposition of the track in the hadron calorimeter is estimated from the momentum measurement in the TEC and energy in the BGO [5]. The excess of energy deposition in the HCAL with respect to this estimate could be due to the presence of K^0; in order to suppress fluctuations, which are proportional to $\sqrt{P_\pi}$, a cut of 5 $(\mathrm{GeV})^{1/2}$ is applied in the ratio $\Delta E_{\mathrm{HC}}/\sqrt{P_\pi}$, where $\Delta E_{\mathrm{HC}} = E_{\mathrm{HC}}^{\mathrm{tot}} - E_{\mathrm{HC}}^{\pi^-}$. Figure 1 shows the distribution of this variable, and the hatched area corresponds to the contribution of the $\nu_\tau\pi^-\bar{\mathrm{K}}^0$, $\nu_\tau\mathrm{K}^-\mathrm{K}^0$, $\nu_\tau\pi^-\pi^0\bar{\mathrm{K}}^0$, $\nu_\tau\pi^-\pi^0\bar{\mathrm{K}}^0$, $\nu_\tau\mathrm{K}^-\pi^0\mathrm{K}^0$ modes.

After this cut the contamination from non-τ sources becomes negligible, and the dominant backgrounds are from τ decays into ρ and a_1, with π^0 leaking from the BGO to the hadron calorimeter. This background is further suppressed by requiring the energy in the first three HCAL layers ($18X_0$) to be less than 0.8 of the total energy deposition in the HCAL. Figure 2 shows the distribution of the fraction of energy measured in these first three layers, after having applied the

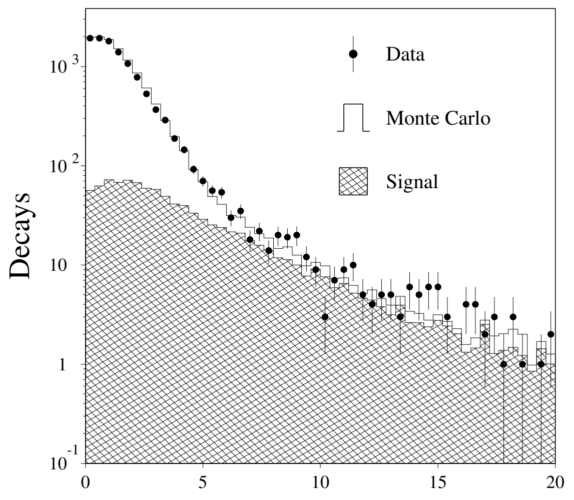

Figure 1.
Distribution of the ratio $\Delta E_{\rm HC}/\sqrt{P_\pi}$ for the preselected τ decays.

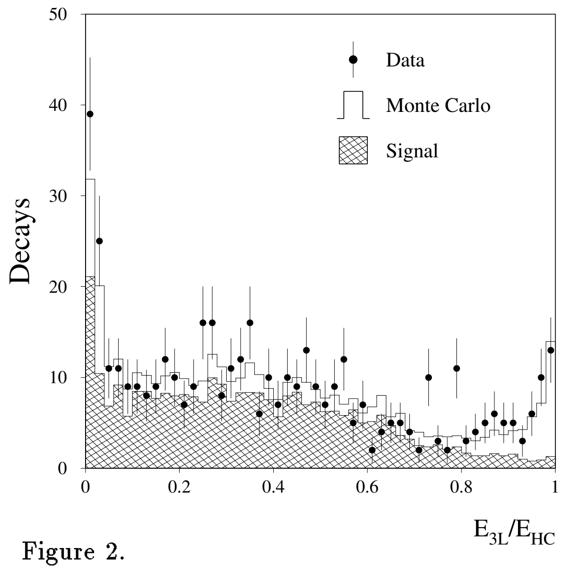

Figure 2.
The distribution of the fraction of the HCAL energy deposited in the first three layers, for decays which passed the cut on the ratio $\Delta E_{\rm HC}/\sqrt{P_\pi}$.

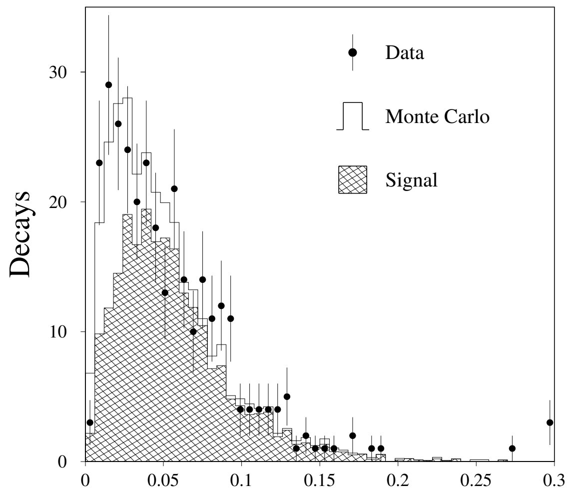

Figure 3.
The distribution of the angle between the charged and the neutral hadron, for decays which survived the two previous cuts.

cut on the ratio $\Delta E_{\rm HC}/\sqrt{P_\pi}$.

To further improve the purity of the selected sample, a cut is applied on the opening angle between the neutral and the charged hadron. For this purpose, their angular separation $\alpha_{\pi^- {\rm K}^0}$ is estimated from the relative position of the HCAL cluster and the impact point of the track in the HCAL. The distribution of the angular separation, for decays which survived the previous cuts, is shown in figure 3; decays are required to be in the range [0.03-0.2] rad.

With the procedure described above, 247 candidate decays are selected, with 27.7 decays expected from the modes without $\rm K^0$. The efficiencies for the signal in the fiducial volume have been estimated with the KORALZ 4.0 Monte Carlo program [6], and their values are the following:

$\tau^- \to \nu_\tau \pi^- \bar{\rm K}^0$	13.0%
$\tau^- \to \nu_\tau {\rm K}^- {\rm K}^0$	5.3%
$\tau^- \to \nu_\tau \pi^- \pi^0 \bar{\rm K}^0$	8.8%
$\tau^- \to \nu_\tau {\rm K}^- \pi^0 {\rm K}^0$	3.7%
$\tau^- \to \nu_\tau \pi^- {\rm K}^0 \bar{\rm K}^0$	19.8%

In the selected $\rm K^0$ sample there is a 68% and 32% component of $\rm K^0_L$ and $\rm K^0_S$, respectively. The modes with charged kaons have significantly lower efficiency than the corresponding modes with charged pions due to the different energy sharing between the charged and neutral hadron; in the K^-K^0 final state the energy is on average divided equally between them, and this leads to small values of the ratio $\Delta E_{HC}/\sqrt{P_\pi}$.

Classification of the Decay

In order to distinguish $\tau^- \rightarrow \nu_\tau \pi^- \bar{K}^0$ decays from $\tau^- \rightarrow \nu_\tau \pi^- \pi^0 \bar{K}^0$ and $\tau^- \rightarrow \nu_\tau \pi^- K^0 \bar{K}^0$ decays, the selected decays are classified into three categories.

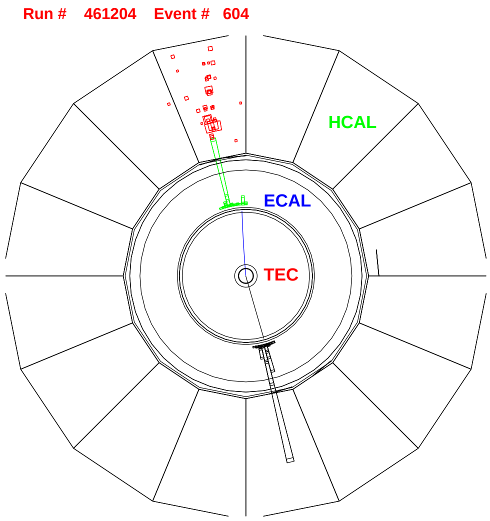

Figure 4.
A $\tau^- \rightarrow \nu_\tau \pi^- \pi^0 \bar{K}^0$ candidate decay.

First of all, decays with a π^0 candidate are selected and classified as $\nu_\tau \pi^- \pi^0 \bar{K}^0$ candidates. In order to fall into this category, the decay must contain an energy cluster in the ECAL of greater than 6 GeV, with a transverse shower shape consistent with the one of a π^0. A typical candidate is shown in Figure 4; in the upper hemisphere, a charged track of 1.36 GeV/c is well separated in space both from the 12.0 GeV π^0 and from the 12.6 GeV neutral hadron shower.

The second category contains decays with additional neutral hadronic energy, which are classified as $\nu_\tau \pi^- K^0 \bar{K}^0$ candidates. The two high energy hadronic showers from a $K^0\bar{K}^0$ pair are usually separated in depth, even not being separated in angle. They are characterized by more even energy deposition than a single neutral hadronic shower. Therefore the decays are classified in this category if at least 10% of the total deposited energy is present in the BGO as well as in the front and deep parts of the HCAL. Figure 5 shows, for example, the fraction of HCAL energy deposited in the front part of the calorimeter; the decays with two neutral kaons contain a more uniform distribution of the energy in the HCAL, with respect to other modes. Figure 6 shows a typical candidate for this category. The candidate decay is shown in the upper hemisphere, which contains a charged track of 2.39 GeV/c, a 9.4 GeV cluster in the BGO and an HCAL neutral hadron shower of 33.6 Gev. The neutral hadron shower has two distinct local maxima, of about 12 GeV and 20 GeV in the front and back part of the HCAL, respectively. In addition the shower shape of the neutral energy cluster in the BGO is not consistent with being a π^0.

The third category contains the decays which

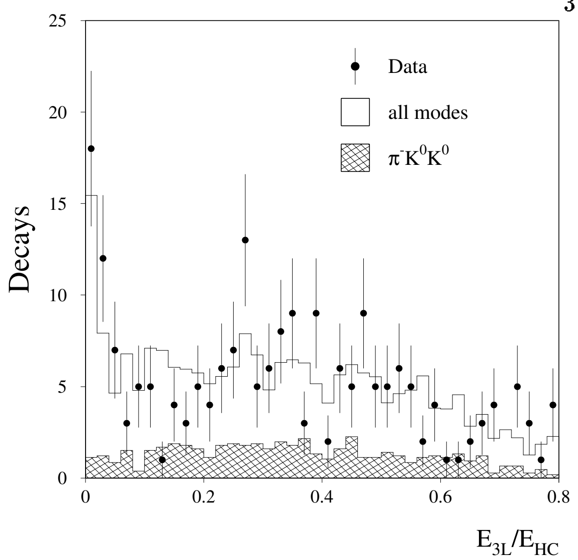

Figure 5.
Fraction of the HCAL energy deposited in the first three layers for $\tau^- \rightarrow \nu_\tau \pi^- K^0 \bar{K}^0$ (hatched area) and all other τ decays.

are not classified in any of the previous two, and are therefore candidates for the $\nu_\tau\pi^-\bar{\mathrm{K}}^0$ mode.

Determination of the Branching Ratios

For each category, the total number of decays is a linear combination of the signal and background channels. The contribution to the signal comes from the modes $\nu_\tau\pi^-\bar{\mathrm{K}}^0$, $\nu_\tau\mathrm{K}^-\mathrm{K}^0$, $\nu_\tau\pi^-\pi^0\bar{\mathrm{K}}^0$, $\nu_\tau\mathrm{K}^-\pi^0\mathrm{K}^0$, and $\nu_\tau\pi^-\mathrm{K}^0\bar{\mathrm{K}}^0$. Anyhow only the branching fractions for the modes without charged kaons are allowed to vary in the fit, while the others are fixed to the values from the ALEPH measurements [7]: $\mathcal{B}(\tau^- \to \nu_\tau\mathrm{K}^-\mathrm{K}^0) = 0.0029 \pm 0.0012$ and $\mathcal{B}(\tau^- \to \nu_\tau\mathrm{K}^-\pi^0\mathrm{K}^0) = 0.0005 \pm 0.0005$.

In order to increase the separation power between the channels, the coefficients of the linear combination are fit to a 10-bin histogram of the π^0 energy for the first category and a 5×3 binned histogram of total decay energy versus invariant mass for the other two categories. A binned maximum likelihood function, which accounts for the finite statistics both in the data and in the Monte Carlo, is used.

The spectrum used for the fit of the $\nu_\tau\pi^-\pi^0\bar{\mathrm{K}}^0$ sample is shown in Figure 7a together with the best fit Monte Carlo distributions. The projections exhibiting the separation between dominant channels for the $\nu_\tau\pi^-\mathrm{K}^0\bar{\mathrm{K}}^0$ and $\nu_\tau\pi^-\bar{\mathrm{K}}^0$ samples are shown in Figures 4b and 4c , respectively, together with the best fit Monte Carlo distributions.

The number of decays expected from the different channels is shown in Table 1 together with the corresponding number of data decays. The numbers of expected decays in each category from the fit are:

$$
\begin{aligned}
\mathrm{N}(\tau^- \to \nu_\tau\pi^-\bar{\mathrm{K}}^0) &= 112.0 \pm 17.7 \\
\mathrm{N}(\tau^- \to \nu_\tau\pi^-\pi^0\bar{\mathrm{K}}^0) &= 33.1 \pm 9.7 \\
\mathrm{N}(\tau^- \to \nu_\tau\pi^-\mathrm{K}^0\bar{\mathrm{K}}^0) &= 55.8 \pm 21.4
\end{aligned}
$$

and the correlation coefficients between the fitted channels are

$$
\begin{aligned}
\rho(\pi^-\bar{\mathrm{K}}^0, \pi^-\pi^0\bar{\mathrm{K}}^0) &= 0.01 \\
\rho(\pi^-\bar{\mathrm{K}}^0, \pi^-\mathrm{K}^0\bar{\mathrm{K}}^0) &= 0.68 \\
\rho(\pi^-\pi^0\bar{\mathrm{K}}^0, \pi^-\mathrm{K}^0\bar{\mathrm{K}}^0) &= 0.36 \ .
\end{aligned}
$$

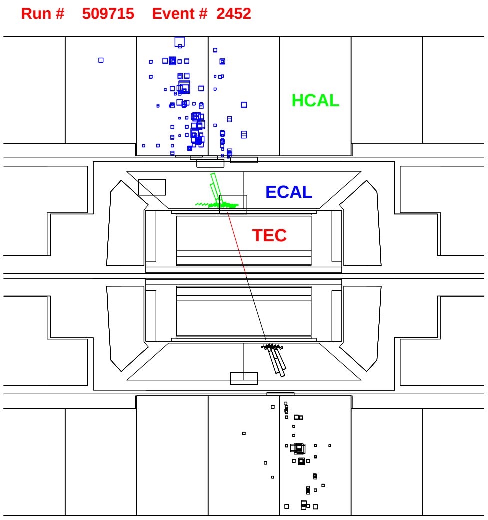

Figure 6.
A $\tau^- \to \nu_\tau\pi^-\mathrm{K}^0\bar{\mathrm{K}}^0$ candidate decay.

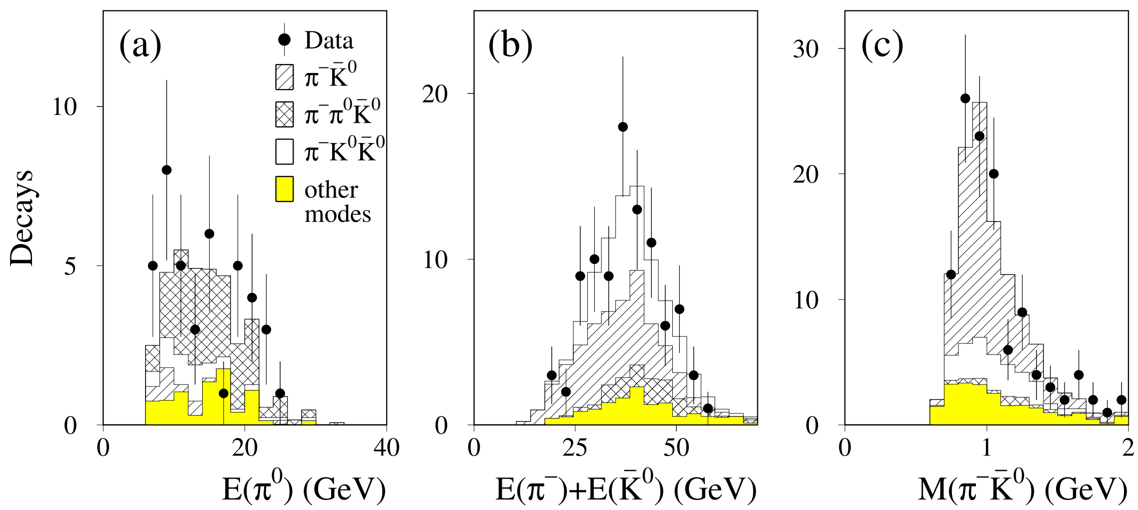

Figure 7.
(a) The spectrum of the π^0 energy for the sample enriched with $\tau^- \to \nu_\tau \pi^- \pi^0 \bar{K}^0$ decays. (b) The spectrum of the sum of energies of the observed τ decay products for the sample enriched with $\tau^- \to \nu_\tau \pi^- K^0 \bar{K}^0$ decays. (c) The invariant mass spectrum of the $\pi^- \bar{K}^0$ system for the sample enriched with $\tau^- \to \nu_\tau \pi^- \bar{K}^0$ decays.

Table 1.
Number of decays detected in the three samples along with the best fit Monte Carlo expectations.

	$\pi^- \bar{K}^0$ sample	$\pi^- \pi^0 \bar{K}^0$ sample	$\pi^- K^0 \bar{K}^0$ sample	Total
Data	114	41	92	247
$\tau^- \to \nu_\tau \pi^- \bar{K}^0$	71.9	2.4	37.7	112.0
$\tau^- \to \nu_\tau K^- K^0$	10.0	0.1	3.8	13.9
$\tau^- \to \nu_\tau \pi^- \pi^0 \bar{K}^0$	3.5	20.3	9.3	33.1
$\tau^- \to \nu_\tau K^- \pi^0 K^0$	0.4	0.3	1.0	1.7
$\tau^- \to \nu_\tau \pi^- K^0 \bar{K}^0$	18.9	4.9	32.0	55.8
Background	11.8	7.5	8.4	27.7
MC total	116.5	35.5	82.2	244.2

Systematic Uncertainties

There are three sources of dominant systematic errors affecting the measurements: they come from the uncertainties in the absolute energy calibration and detector resolution functions, from the uncertainties in the background estimation, and from the theoretical uncertainties.

The calibration uncertainties affect both the selection efficiency and the shape of the final distributions used for the fit. For what concerns the BGO, the accuracy in the energy scale for electrons and photons is estimated to be 1% at 1 GeV from the measurement of the position of the π^0 mass peak and 0.1% at 45 GeV from a study of $Z \rightarrow e^+e^-(\gamma)$ events. The momentum scale of the TEC is verified to 1% accuracy from 1 to 45 GeV using low energy electrons as well as muons from τ and Z decays. The absolute energy scales of the BGO and HCAL for hadrons are each known to 1.5% in the central region from the position of the ρ mass peak. Table 2 shows the uncertainties in the number of signal decays due to each of these absolute energy calibrations.

The resolution function of the HCAL is verified using test beam data (figure 8) and $\tau^- \rightarrow \rho^-\nu_\tau$ decays (figure 9). No discrepancy between data and Monte Carlo is observed within the achieved statistical errors, limiting possible uncertainty of the non-K^0 background to ± 2.1 decays.

The systematic error due to the uncertainty in the rate of the decay modes with charged kaons is estimated varying their branching fractions according to the uncertainties quoted in reference [7]. If the number of K^-K^0 decays is left free in the fit to the data, the formal result is $\mathcal{B}(\tau^- \rightarrow \nu_\tau K^-K^0) = 0.0023 \pm 0.0045$; this result represents an additional cross-check and shows consistency with the result which is actually used to estimate the systematic error. The uncertainty in the number of π^0's from $\tau^- \rightarrow \rho^-\nu_\tau$ and $\tau^- \rightarrow a_1^-\nu_\tau$ decays leaking to the HCAL also affects the measurement. The net effect is estimated using decays with abnormally high energy deposition in the first three layers of the HCAL (these events are not used in the fit). This uncertainty is estimated to be 20% of the number of $\tau^- \rightarrow \rho^-\nu_\tau$ and $\tau^- \rightarrow a_1^-\nu_\tau$ decays predicted by Monte Carlo simulation.

Since the selection efficiency is not uniform over the phase space, an uncertainty in the measurement comes from the uncertainty in the matrix element for the τ decays into three particles with one or two kaons. In the Monte Carlo program [8] used to simulate τ decays, the assumption is made that these decays proceed through axial hadronic current and lowest resonances. These assumptions have been varied, in order to estimate the corresponding uncertainty in the efficiencies; the result is shown in table 2. An additional systematic error comes from the uncertainty in the CP phase of the $K^0\bar{K}^0$ system in the decay

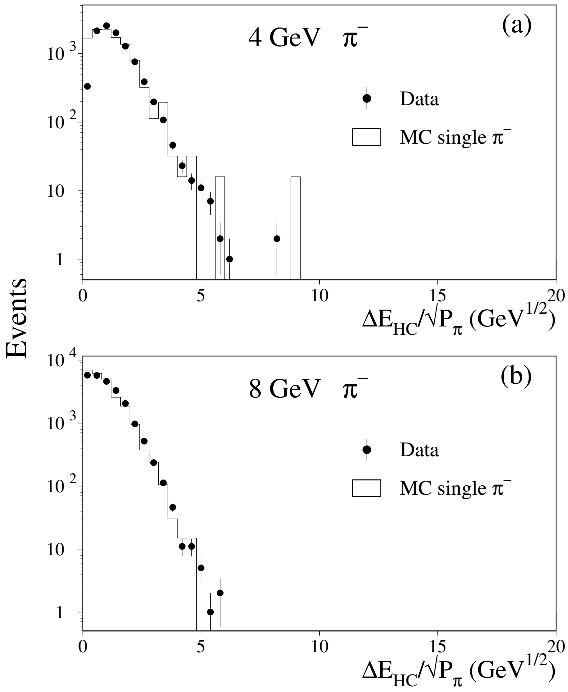

Figure 8.
The spectra of the ratio $\Delta E_{\mathrm{HC}}/\sqrt{P_\pi}$ for (a) 4 GeV and (b) 8 GeV single pions as measured in the test-beam (dots) and predicted by the Monte Carlo (solid histogram).

Table 2.
Summary of the systematic uncertainties in the numbers of fitted decays.

Source		$\Delta N_{\pi^-\bar{K}^0}$	$\Delta N_{\pi^-\pi^0\bar{K}^0}$	$\Delta N_{\pi^-K^0\bar{K}^0}$
	HCAL	3.5	0.9	4.3
Calibration	ECAL	1.0	1.6	2.5
	TEC	1.0	0.8	0.6
	π^0	2.0	0.8	0.6
Background	$\pi^\pm/K^\pm$	1.5	0.5	0.6
	$\Delta N_{K^-K^0}$	3.4	0.2	2.4
	$\Delta N_{K^-\pi^0K^0}$	0.2	0.8	0.9
Theory	matrix element	3.9	1.2	4.0
	$CP(K^0\bar{K}^0)$	-	-	2.7
Total	ΔN^{syst}	6.9	2.6	7.4

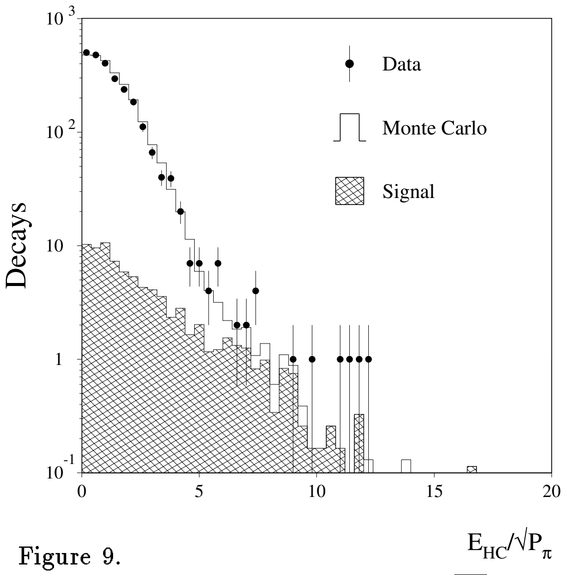

Figure 9.
The distribution of the ratio $\Delta E_{\rm HC}/\sqrt{P_\pi}$ for the decays $\tau^- \to \rho^-\nu_\tau$ as observed in data (dots) and predicted by the Monte Carlo (solid histogram). The shaded area represents the contribution of τ decays with neutral kaons.

$\tau^- \to \nu_\tau\pi^-K^0\bar{K}^0$. The error is estimated from the change in the result when assuming that the $K^0\bar{K}^0$ sample consists of only CP-odd or only CP-even components. For the central value of the measured branching fraction, the following proportion is assumed $K_LK_L : K_SK_S : K_SK_L = 0.25 : 0.25 : 0.5$.

The different contributions to the systematic errors for the number of fitted decays are shown in table 2. In the combination of the systematic errors from different sources, it is assumed that there are no correlations among them.

Final Results

The following final results are obtained for the branching fractions:

$$\mathcal{B}(\tau^- \to \nu_\tau\pi^-\bar{K}^0) = 0.0095 \pm 0.0015 \pm 0.0006$$
$$\mathcal{B}(\tau^- \to \nu_\tau\pi^-\pi^0\bar{K}^0) = 0.0041 \pm 0.0012 \pm 0.0003$$
$$\mathcal{B}(\tau^- \to \nu_\tau\pi^-K^0\bar{K}^0) = 0.0031 \pm 0.0012 \pm 0.0004$$

where the first and second errors are statistical and systematic, respectively.

The invariant mass spectrum of the $\pi^-\bar{K}^0$ system is in qualitative agreement with the model assuming that this decay proceeds through the chain $\tau^- \to \nu_\tau K^{*-} \to \nu_\tau\pi^-\bar{K}^0$. If we assume that there are no other contributions to the final state $\nu_\tau\pi^-\bar{K}^0$, we can extract

$$\mathcal{B}(\tau^- \to \nu_\tau K^{*-}) = 0.0142 \pm 0.0022 \pm 0.0009$$

where the errors are statistical and systematic, respectively.

If conversely we assume the existence of this final state produced from continuum or high mass resonances, and include these modes in the fit to our data, upper limits can be put to this production modes. For the $K^{*-}(1430)$ resonance the following limit is obtained:

$$\mathcal{B}(\tau^- \to \nu_\tau \pi^- \bar{K}^0)_{\rm nonresonant} < 0.0017 \quad 95\% \text{ CL},$$

while for the non-resonant contribution:

$$\mathcal{B}(\tau^- \to \nu_\tau \pi^- \bar{K}^0)_{K^{*-}(1430)} < 0.0011 \quad 95\% \text{ CL}.$$

It must be underlined that, even if there is no explicit identification of the charged hadron, these measurements of the branching fractions are largely independent of the assumed branching fractions for $\tau^- \to \nu_\tau K^- K^0$ and $\tau^- \to \nu_\tau K^- \pi^0 K^0$. This is due to the fact that the selection efficiencies for these modes are significantly lower than the corresponding efficiencies for modes with charged pions, $\tau^- \to \nu_\tau \pi^- \bar{K}^0$ and $\tau^- \to \nu_\tau \pi^- \pi^0 \bar{K}^0$, as a result of the different kinematics of these decays. In addition, the measurement of the branching fraction $\mathcal{B}(\tau^- \to \nu_\tau \pi^- K^0 \bar{K}^0)$ is insensitive to the theoretical assumptions on the matrix element and the CP phase of the $K^0\bar{K}^0$ system.

REFERENCES

1. E. Mirkes, presentation at this workshop.
2. L3 Collaboration, M. Acciarri *et al.*, *Phys. Lett.* **B352** (1995) 487.
3. L3 Collaboration, B. Adeva *et al.*, *Nucl. Instr. and Meth.* **A289** (1990) 35;
   O. Adriani *et al.*, *Nucl. Instr. and Meth.* **A302** (1991) 53;
   K. Deiters *et al.*, *Nucl. Instr. and Meth.* **A323** (1992) 162;
   J. A. Bakken, *Nucl. Instr. and Meth.* **A275** (1989) 81.
4. A. Arefiev *et al.*, *Nucl. Instr. and Meth.* **A251** (1986) 258;
   A. Arefiev *et al.*, *Nucl. Instr. and Meth.* **A285** (1989) 403.
5. L3 Collaboration, O.Adriani *et al.*, *Phys. Lett.* **B294** (1992) 466;
   L3 Collaboration, O.Acciarri *et al.*, *Phys. Lett.* **B341** (1994) 245.
6. S. Jadach, B.F.L. Ward and Z. Wąs, *Comp. Phys. Comm.* **66** (1991) 276;
   R. Kleiss *et al.*, in "Z Physics at LEP1", CERN Report CERN 89-08 (1989), Vol. 3, p. 1.
7. ALEPH Collaboration, D. Buskulic *et al.*, *Phys. Lett.* **B332** (1994) 219.
8. S. Jadach *et al.*,, *Comp. Phys. Comm.* **76** (1994) 361;
   S. Jadach, J.H. Kühn and Z. Wąs, *Comp. Phys. Comm.* **64** (1991) 275.